

PAPER • OPEN ACCESS

Berreman-assisted optical characterization of sub-percolation threshold, ultrathin near-zero-index films

To cite this article: Luke A Herman *et al* 2025 *J. Phys. Photonics* **7** 025009

View the [article online](#) for updates and enhancements.

You may also like

- [Broadband near-zero index metamaterials](#)
K Konstantinidis and A P Feresidis
- [Three-wave mixing experiments in indium–tin–oxide thin-films with no phase matching](#)
Kyle Wynne, Marjan Bazian and Mark C Harrison
- [A novel surface-integral-equation formulation for efficient and accurate electromagnetic analysis of near-zero-index structures](#)
Hande bili, Yeim Koyaz, Utku Özmü et al.



PAPER

OPEN ACCESS

RECEIVED
29 August 2024REVISED
15 January 2025ACCEPTED FOR PUBLICATION
26 January 2025PUBLISHED
25 February 2025

Original content from
this work may be used
under the terms of the
[Creative Commons
Attribution 4.0 licence](#).

Any further distribution
of this work must
maintain attribution to
the author(s) and the title
of the work, journal
citation and DOI.



Berreman-assisted optical characterization of sub-percolation threshold, ultrathin near-zero-index films

Luke A Herman , Jie Hu and Zhaowei Liu*

Department of Electrical and Computer Engineering, University of California, San Diego, 9500 Gilman Drive, La Jolla, CA 92093, United States of America

* Author to whom any correspondence should be addressed.

E-mail: zhaowei@ucsd.edu**Keywords:** epsilon-near-zero, near-zero-index, tunable, ultrathin film, integrated photonics, optical characterization, electrical characterization

Abstract

Due to its transparent and conductive nature, indium tin oxide (ITO) offers substantial benefits in several industries, such as thin film transistors, displays, and nanophotonics. Previous studies on ultrathin ITO have so far focused on its electrical properties but have neglected the technologically important epsilon-near-zero (ENZ) optical features due to the difficulty of extracting the refractive index and the thickness-dependent degradation of the optical properties. Here, we demonstrate a complementary metal-oxide-semiconductor (CMOS)-compatible deposition procedure for sub-percolation thickness (below 4 nm) ITO using a dry-etch assisted radiofrequency magnetron sputtering technique that yields continuous films in a precisely controlled manner. Through interface engineering and post-deposition annealing optimization, we show that these ITO films can retain high carrier mobility ($43 \text{ cm}^2 \text{ V}^{-1} \text{ s}^{-1}$) while achieving a tunable near-zero-index (NZI) regime throughout the telecommunications band using a Berreman-assisted optical characterization technique. Our result opens the possibility of efficiently designing ENZ/NZI materials at the nanoscale using a robust fabrication approach for applications in nanophotonics.

1. Introduction

Materials that can be characterized as possessing free charge carriers, such as metals and highly doped semiconductors, have a special regime where the real permittivity of the material approaches zero, denoted as the epsilon-near-zero (ENZ) regime [1, 2]. There is significant interest in this class of materials, as they display a variety of exotic optical effects, such as sub-picosecond near-unity refractive index change [3], harmonic generation enhancement [4], and slow-light effects [5]. Transparent conducting oxides, e.g. indium tin oxide (ITO), aluminum-doped zinc oxide [6], have garnered substantial attention as these materials exist within a sub-class of ENZ materials, i.e. near-zero-index (NZI) due to their low-loss within their ENZ regime [7]. Recently, there has been a push at miniaturizing ITO films [8] due to pronounced thickness-dependent electric field enhancements [9] and enhanced second-order nonlinear optical enhancements [10]; however, scattering-induced losses [11] largely push these films out of NZI, which limits the viability for photonic applications. Additionally, optical characterization of ultrathin films ($< 10 \text{ nm}$) becomes challenging, as traditional refractive index extraction methods, such as ellipsometry [12] and reflection/transmission/absorption spectroscopy [13], fail due to the absence of spectral features and low optical path length.

Ultrathin ITO films have been mainly investigated for use as an active layer in thin film transistor technologies. Currently, these films are fabricated using various fabrication techniques, such as atomic layer deposition [14], molecular beam epitaxy (MBE) [15], RF magnetron sputtering [16], and 2D liquid metal printing [17]. While several of these methods showcase films grown with thicknesses lower than 4 nm [14, 15], the electrical performance is significantly reduced due to nano-islands forming instead of a continuous film. Recently, Si *et al* [18] have shown that through a sputtering and wet etch approach, sub-percolation ITO

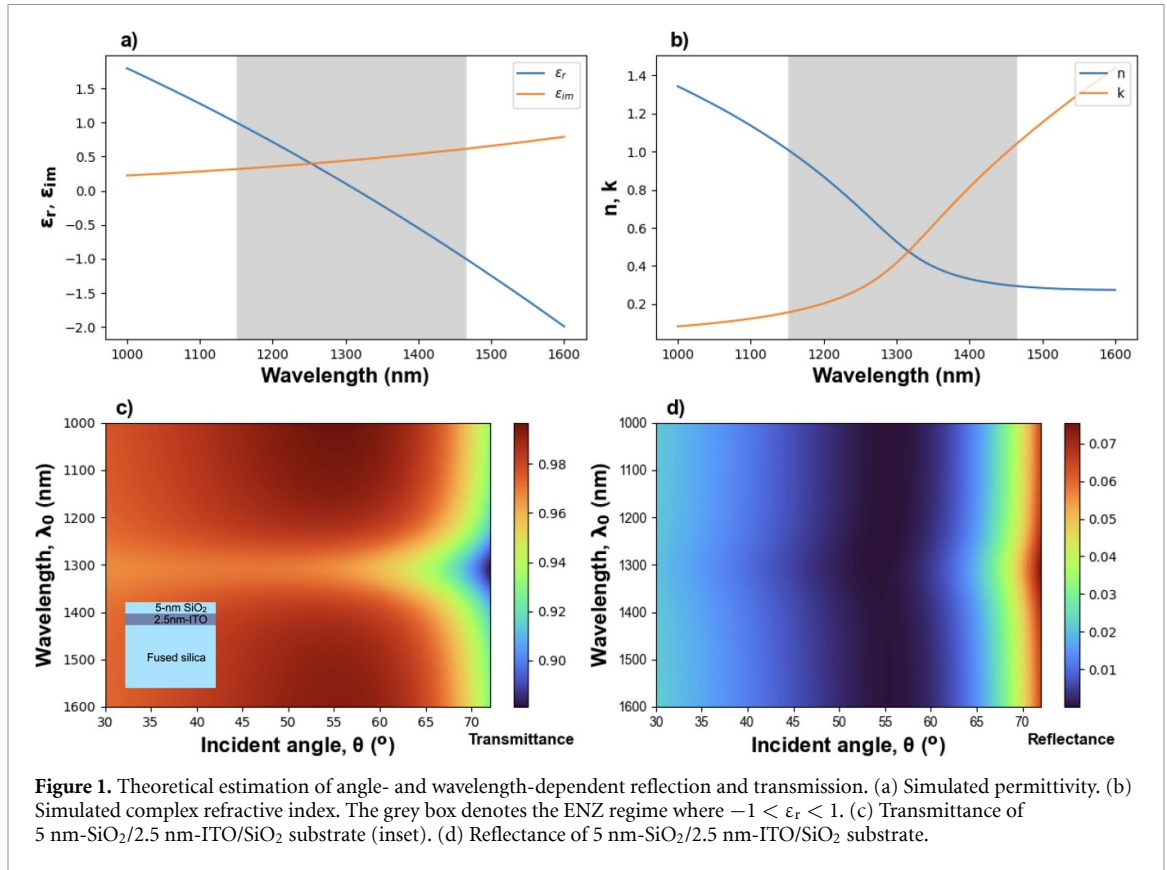


Table 1. Simulated ITO parameters based on the Drude model.

ω_p (eV)	Γ_p (eV)	ϵ_∞	t_{ITO} (nm)
1.94	0.09	3.8	2.5

continuous films can be successfully fabricated. However, due to the wet etching process, the surface roughness of their films is roughly on the order of the thickness of the sample, which results in highly non-uniform films. Reactive ion etching (RIE) on the other hand, offers highly anisotropic etching, precise control of etching parameters, and is compatible with other vacuum-based fabrication steps [19].

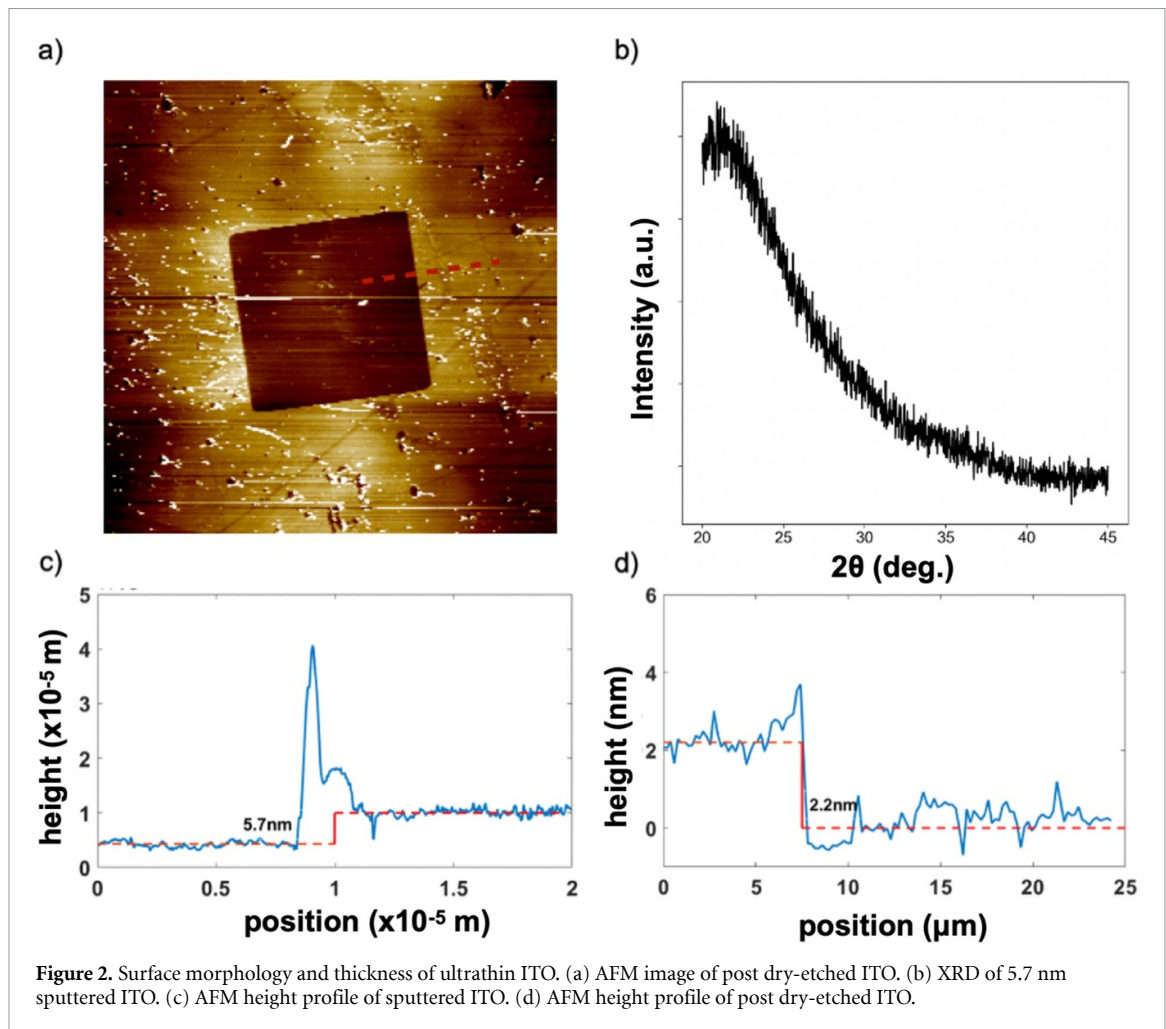
In this study, we first propose a CMOS-compatible fabrication method that enables ITO film thicknesses below the percolation threshold using an RF magnetron sputtering and dry-etch RIE approach. We then elucidated the film's optical properties using a Berreman-assisted characterization method [20]. Finally, through interface engineering and post-deposition annealing, we demonstrated an NZI regime within ultrathin ITO, overcoming the problem of thickness-dependent increase in optical loss [11]. We believe this approach offers new flexibility in the design of NZI metamaterials, as the decreased dimensionality provides intriguing possibilities [9], such as NZI-coupled inter-subband transition engineering for enhanced nonlinear optical applications.

2. Theory

In the near-infrared spectrum, bulk ITO, as a degenerately doped semiconductor, can be theoretically modeled using the standard Drude–Lorentz model [21] given by the following equation:

$$\epsilon_{ITO}(\omega) = \epsilon_\infty - \frac{\omega_p^2}{\omega^2 + i\Gamma_p\omega}, \quad (1)$$

where ω_p is the plasma frequency, Γ_p is the associated damping factor, and ϵ_∞ is the high-frequency permittivity contribution. One can see that at a particular frequency ω_{ENZ} , the real part of the permittivity vanishes. At this ENZ crossover point, it has been shown that ultrathin ($< \lambda/50$) films support radiative and non-radiative optical polariton modes [22–24] that provide large field enhancements due to the boundary conditions of Maxwell's equations, where $\mathbf{E}_{\perp,2} = \left(\frac{\epsilon_1}{\epsilon_2}\right) \mathbf{E}_{\perp,1}$. Specifically, the radiative optical polariton



mode, named the Berreman mode [25], appears due to the excitation of a leaky mode inside the light cone of a three-layered dielectric/ENZ layer/dielectric structure [26]. Due to its radiative nature, the mode is accessible without k -vector matching methods, such as grating- or prism-coupling [26]. Additionally, when the thickness of these materials is significantly reduced into the ultrathin regime, the mode's dispersion becomes flat in nature [27], leading to large electric field confinement within the medium.

Figure 1 showcases the simulated angle-dependent, wavelength-dependent reflection and transmission from an ultrathin ITO film, where the film's material properties are modeled using the Drude-Lorentz model and the parameters [28] are as follows in table 1.

Figures 1(a) and (b) show the ITO's complex permittivity and refractive index respectively. The shaded area in figures 1(a) and (b) denotes the ENZ regime, which is defined as $-1 < \epsilon_r < 1$. In figure 1(b), the imaginary part of the refractive index within the ENZ regime is less than unity: this demonstrates ITO's NZI feature. As can be seen in figure 1(c), a radiative Berreman mode is manifested at λ_{ENZ} due to the presence of a transmission (absorption) dip (peak). Additionally, its broadband nature in k -space can be visibly seen due to its angle-independent prominence. Due to the non-zero imaginary part in the permittivity (figure 1(a)), the strength of the polaritonic resonance is significantly reduced.

3. Results

The ultrathin ITO films were first fabricated through radiofrequency (RF) magnetron sputtering [29] by adopting Li *et al*'s [16] deposition parameters and dry-etched through a RIE machine in an argon environment (see materials and methods section for detailed fabrication). Figure 2 details the pre-etched surface morphology and the thickness of pre/post-etched ITO films. To determine the film's structural morphology, we perform x-ray diffraction (XRD) (figure 2(b)) measurements (see materials and methods for experimental details). Specifically, the absence of peaks in the XRD experimental dataset showcases the amorphous nature of the ITO films. We then perform atomic force microscopy (AFM) to determine the thickness of ITO pre- and post-dry etching process. Figure 2(c) showcases the AFM measurement of the pre-etched ITO layer. As we can see, an ITO layer of 5.7 nm was fabricated, where the root mean square

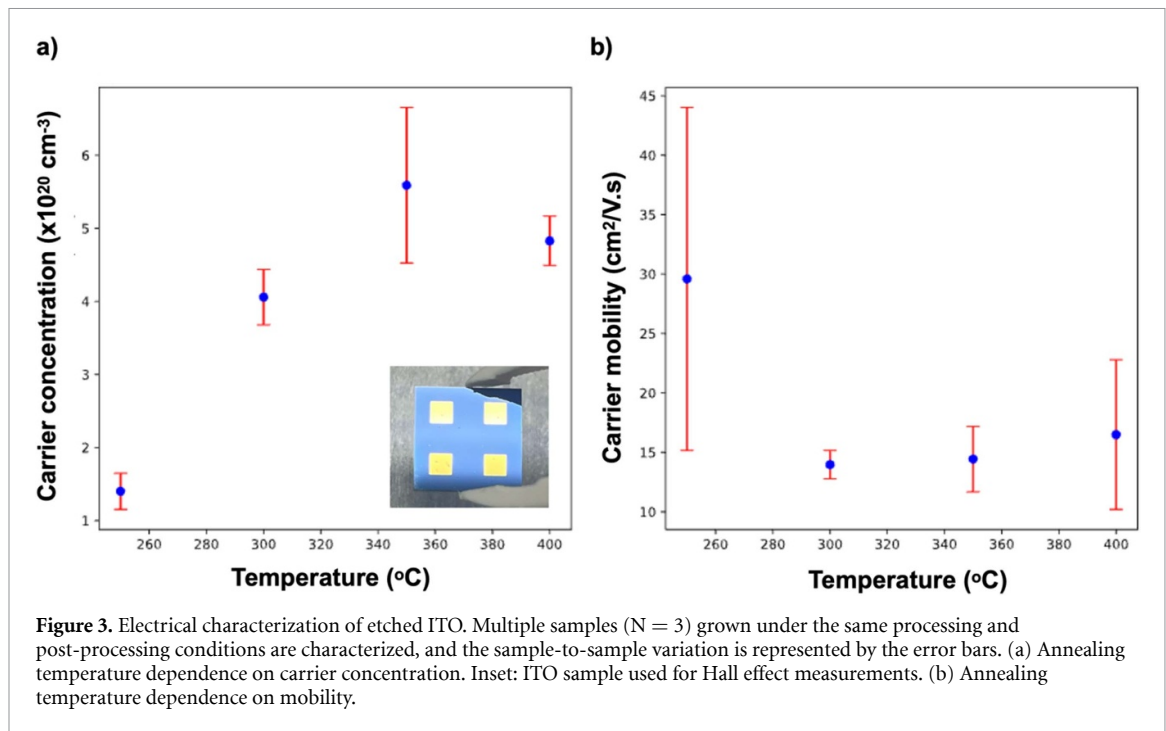


Figure 3. Electrical characterization of etched ITO. Multiple samples ($N = 3$) grown under the same processing and post-processing conditions are characterized, and the sample-to-sample variation is represented by the error bars. (a) Annealing temperature dependence on carrier concentration. Inset: ITO sample used for Hall effect measurements. (b) Annealing temperature dependence on mobility.

(RMS) roughness of 0.65 nm showcases the ultrasmooth ITO nanolayer. The spike can be attributed to a combination of the edge spiking effect of sputtering onto a patterned area [30] (*see materials and methods section for etch rate determination*) and edge overshoot AFM artifact [31]. After dry etching at a rate of 2 nm min^{-1} , the AFM measurements show the formation of an ultrathin film of 2.2 nm (figure 2(d)). Additionally, the ITO film's post-etched RMS of 0.36 nm showcases that the ITO retains its atomically smooth nature.

3.1. Electrical characterization

ITO's optical properties are known to be highly tunable through tuning deposition parameters [32], as well as through tuning post-deposition annealing treatment methods [33]. Due to its Drude-like response in the near-infrared, we can analyze the electrical properties of ITO to determine the plasma frequency $\omega_p = \sqrt{\frac{ne^2}{\epsilon_0 m^*}}$ and the damping factor $\Gamma_b = \frac{e}{\mu m^*}$ where n is the carrier concentration in cm^{-3} , μ is the carrier mobility in $\text{cm}^2 \text{ V}^{-1} \text{ s}^{-1}$, e is the elementary charge, ϵ_0 is the permittivity of free space, and m^* is the electron effective mass. A series of Hall effect measurements were undertaken to analyze the dependence of annealing temperature on ITO's electrical properties. The amorphous ITO samples were annealed in a nitrogen-rich atmosphere to simultaneously promote the growth of large crystalline domains [34], which increases carrier mobility, and to increase oxygen-vacancies, which increases the carrier concentration. Figure 3 showcases the annealing temperature dependence on the electrical properties of ITO. From figure 3(a), a clear trend is seen, as the carrier concentration increases with annealing temperature until it reaches a maximum at 350 °C and drops afterwards. At a certain doping threshold, the carrier concentration is effectively saturated due to excessive ion doping, which impedes free carrier motion by increasing the impurity scattering defects [35]. Figure (b) shows an opposite trend, where the mobility is highest at lower temperatures, and reduces to a quasi-constant value after exceeding temperatures of ~ 300 °C. By increasing annealing temperature, the films change from amorphous structures to a polycrystalline lattice [34]. Above a certain temperature, the increase of polycrystallinity increases the scattering from the grain boundaries, which reduces the overall carrier mobility [36].

The samples annealed at 350 °C offer the best device performances for optical applications, such as a high carrier concentration ($n \sim 5.6 \times 10^{20} \text{ cm}^{-3}$) and an acceptable carrier mobility ($\mu \sim 15 \text{ cm}^2 \text{ V}^{-1} \text{ s}^{-1}$). The low mobility values here can be explained by two main contributions. Firstly, these samples fabricated for electrical measurements had no protection layer; therefore, an electrical dead passivation layer could form at the air-ITO interface [37]. Due to the ~ 2 nm thickness of our samples, an electrically dead layer can dramatically reduce the carrier mobility [37] due to interface defects. For further improvements of the electrical properties, an external passivation layer, such as SiO_2 or Al_2O_3 , could reduce the effect. Second, as these samples were annealed in a N_2 -rich environment, we speculate that oxygen could leak into the

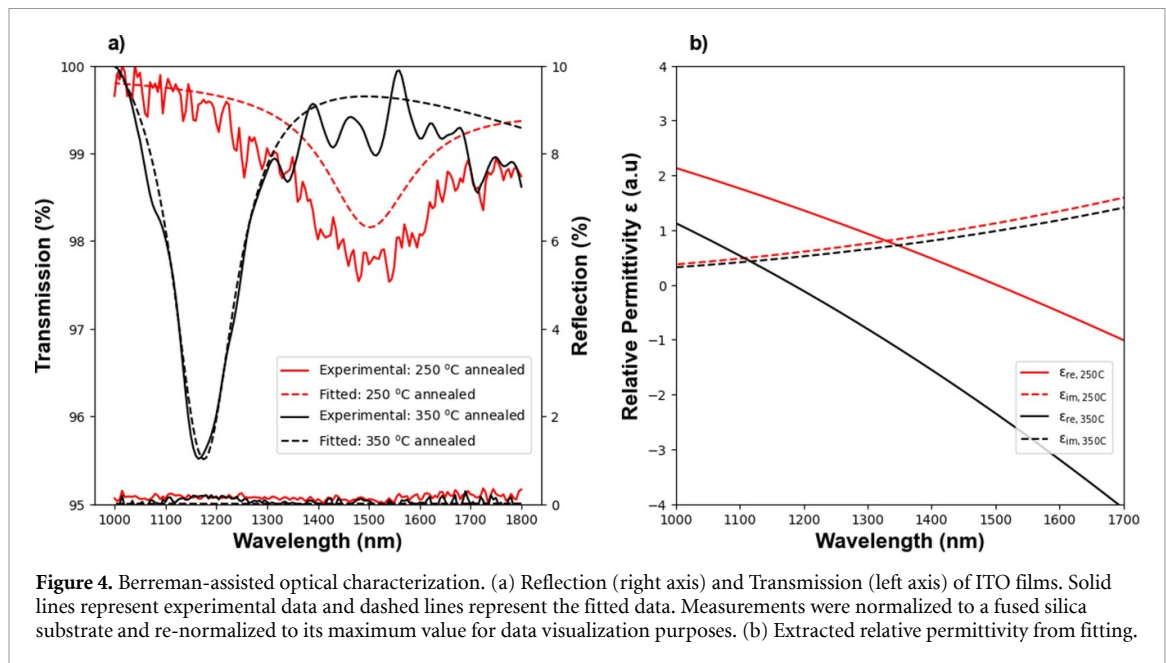


Figure 4. Berreman-assisted optical characterization. (a) Reflection (right axis) and Transmission (left axis) of ITO films. Solid lines represent experimental data and dashed lines represent the fitted data. Measurements were normalized to a fused silica substrate and re-normalized to its maximum value for data visualization purposes. (b) Extracted relative permittivity from fitting.

annealing environment and reduce the overall annealing effect. However, we attribute the first contribution as the dominant physical mechanism, as will be shown in the next section.

3.2. Experimental optical characterization

The most common and accurate experimental method for extracting material optical properties is through spectroscopic ellipsometry [38] (SE), where the ratio of *p*- and *s*- polarization states is gathered at the output as light is reflected at oblique angles from a thin film sample. However, as film thickness decreases below 10 nm, the problem of fitting a material's optical properties becomes ill-posed due to the reduction in optical path length, and due to low spectral signatures [37, 39]. Therefore, a fine-tuned experimental approach is necessary to maximize the experimental conditions where the spectral features are most prominent. To maximize the spectral signatures, we perform reflection/transmission measurements (see materials and methods section for experimental details) of our ultrathin ITO layers at a high-incident angle ($\theta = 50^\circ$) using *p*-polarized light to elucidate the appearance of the Berreman mode and to minimize the sample's reflectance (figure 1).

Figure 4 demonstrates the reflection and transmission, and the extracted relative permittivity of 2.2 nm ITO layers grown with a 5 nm SiO₂ protection layer on top and annealed using the annealing parameters detailed in the previous section. From figure 1(a), the sample annealed at 350 °C provides the largest dip in the transmission spectrum and its resonance is blue-shifted relative to the sample annealed at 250 °C. Additionally, both samples have negligible reflectance ($<0.5\%$) across the whole measured spectrum. Both samples' experimental transmission curves can be well-fitted with theoretical predictions (see materials and methods for fitting methodology).

Previous studies on the thickness-dependence optical properties of ITO [11, 37] demonstrated an inversely proportional relationship of thickness and Γ_b , due to both the increased importance of the non-electrical interface layer and the expansion of percolating nano-islands. However, most of these studies have either avoided using a dielectric protection layer, optimizing the deposition recipe for continuous film growth, or utilizing a post-deposition annealing procedure. In our case, we have significantly reduced the thickness-dependent effects, which can be shown through the strength of the Berreman resonance: through annealing at 350 °C, we obtain a carrier concentration $n \sim 1.16 \times 10^{21} \text{ cm}^{-3}$, and a mobility $\mu \sim 43 \text{ cm}^2 \text{ V}^{-1} \text{ s}^{-1}$, which is remarkable for an ultrathin ITO film. For the case of the film annealed at 250 °C, even though the mobility ($\mu \sim 30 \text{ cm}^2 \text{ V}^{-1} \text{ s}^{-1}$) is quite high, the high optical loss at ENZ ($\epsilon_{im} > 1$) pushes the film out of the NZI range. In addition, the effect of the dielectric protection layer is pronounced. Table 2 outlines the variation of Drude-parameters extracted from electrical characterization (without dielectric protection) vs optical characterization (with dielectric protection), as well as summarizes the existing literature.

Table 2. Summary of ultrathin ITO optical properties for nanophotonic applications.

Deposition method	Characterization method	Post-processing	Dielectric protection	n (10^{20} cm^{-3})	μ ($\text{cm}^2 \text{ V}^{-1} \text{ s}^{-1}$)	$\lambda_{\text{ENZ/NZI}}$ (nm)	t_{ITO} (nm)
RF Sputtering + Dry Etch ^a	Hall effect	1 h, N ₂ , 350 °C	No	5.6	15	—	2.2
RF Sputtering + Dry Etch ^a	Berremman-assisted R/T	1 h, N ₂ , 350 °C	Yes	11.6	43	1175	2.2
PLD [37]	Ellipsometry	No	No	7.9	8	2100	16
Liquid metal [8]	Hall effect	Air, 250 °C	No	1.6	20.3	—	1.8
Electron-beam evaporation [11]	Oblique angle transmission/Hall effect	No	No	10.59	14.96	1255	52

^a This study.

4. Discussion

In summary, ultrathin, continuous ITO films that break the percolation threshold were fabricated using an RF-sputtering and dry-etch approach. A novel method to optically characterize these ultrathin films through a Berremman-assisted methodology revealed high-mobility, high-carrier concentration films with an NZI regime near the technologically important telecommunications O-band. This research is poised to enable new technologies in nanophotonics, such as optical/electrically active metasurfaces [40], hybrid ENZ/silicon integrated photonic circuits [37], 2D heterostructures [41], and nonlinear optics [42].

5. Materials and methods

Material fabrication: In this study, the ITO nanolayers are first grown by radio-frequency magnetron sputtering using a commercial ITO target (90 wt% In₂O₃/10 wt% SnO₂) in an AJA ATC Orion 8 RF Sputtering system on SiO₂/Si (electrical) and fused silica (optical) substrates. The deposition pressure was set to 2 mTorr, the RF power was 150 W, and the deposition temperature was 200 °C. During the deposition, the gas flow ratio of 9 sccm argon/1 sccm O₂ was optimized for amorphous film growth and a deposition rate 3.8 nm min⁻¹. Films were grown with a target thickness of 6 nm in mind, as that thickness exceeds the percolation threshold of ITO [24], where below that specified thickness independent nano-islands are formed instead of continuous thin films. Following sputtering, the samples were dry etched in an Oxford Plasmalab 80 Plus RIE machine for anisotropic etching. The etching pressure was set to 35 mTorr, the power was 50 W and an Argon flow of 25 sccm was used. We optimized the etching rate to be 2 nm min⁻¹. After etching, samples were annealed in a nitrogen-rich environment (N₂ 10 sscm) for one hour in an Allwin21 AccuThermo AW610 Rapid Thermal Process System.

Etch rate determination: After completing the deposition of ITO, we first covered the entire ITO surface with photoresist. Subsequently, we used photolithography to expose an array of 20 μm square patterns with 20 μm spacing, uniformly distributed across the ITO surface. Next, we performed the dry etching process, while the unexposed areas remained protected by the photoresist and were not etched. Following this, the photoresist was removed using Remover PG, and AFM measurements were conducted. At the edges of the exposed squares, where etched and unetched ITO meet, a variation in thickness was observed. This transition region served as the basis for determining the etching rate.

Electrical characterization: DC Hall effect measurements were taken on a LakeShore 8400 Series HMS tool with an excitation magnetic field of 0.8 T and an excitation current of 1 mA. Samples were patterned in a van der Pauw geometry with sputtered Au as the electrode on top of the ITO layers.

Reflection/transmission measurements: Reflection, R , and transmission, T , measurements were measured using a PerkinElmer Lambda 1050+ UV/VIS/NIR Spectrometer. All measured data are calibrated with 0/100% R/T measurements with no samples inside the chamber to reduce experimental noise (~0.5%). The

transfer matrix method was used to fit experimental R/T curves using a Levenberg–Marquardt least-squares algorithm with simulated data using the Drude model as material input.

XRD measurements: XRD measurements were performed in a Panalytical X'Pert x-ray diffractometer in the point-source configuration using Cu-K α radiation generated at a voltage of 45 kV and a tube current of 40 mA. Z-axis height of samples was set carefully using a mechanical depth stop to ensure repeated optimal positioning of a sample's top surface. Samples were scanned over $2\theta = 20\text{--}45^\circ$ with a 0.02° step size in the $2\theta\text{--}\omega$ geometry.

Data availability statement

The data cannot be made publicly available upon publication because no suitable repository exists for hosting data in this field of study. The data that support the findings of this study are available upon reasonable request from the authors.

Acknowledgment

This work is supported by the National Science Foundation, UCSD MRSEC DMR-2011924. This work was performed in part at the San Diego Nanotechnology Infrastructure (SDNI) of University of California, San Diego (UCSD), a member of the National Nanotechnology Coordinated Infrastructure (NNCI), which is supported by the National Science Foundation (Grant ECCS-1542148). The authors have no conflicts of interest to report.

ORCID iDs

Luke A Herman  <https://orcid.org/0000-0001-7198-4527>

Jie Hu  <https://orcid.org/0009-0009-2130-3290>

References

- [1] Wu J, Xie Z T, Sha Y, Fu H Y and Li Q 2021 Epsilon-near-zero photonics: infinite potentials *Photon. Res.* **9** 1616–44
- [2] Liberal I and Engheta N 2017 Near-zero refractive index photonics *Nat. Photon.* **11** 149–58
- [3] Alam M Z, De Leon I and Boyd R W 2016 Large optical nonlinearity of indium tin oxide in its epsilon-near-zero region *Science* **352** 795–7
- [4] Rodriguez-Sune L, Scalora M, Johnson A S, Cojocaru C, Akozbek N, Coppens Z J, Perez-Salinas D, Wall S and Trull J 2020 *APL Photonics* **5** 010801
- [5] Bello F, Page A F, Pusch A, Hamm J M, Donegan J F and Hess O 2017 *Sci. Rep.* **7** 8702
- [6] Caspani L *et al* 2016 Enhanced nonlinear refractive index in ϵ -near-zero materials *Phys. Rev. Lett.* **116** 233901
- [7] Kinsey N, DeVault C, Boltasseva A and Shalaev V M 2019 Near-zero-index materials for photonics *Nat. Rev. Mater.* **4** 742–60
- [8] Tang Y, Huang C-H and Nomura K 2022 Vacuum-free liquid-metal-printed 2D indium–tin oxide thin-film transistor for oxide inverters *ACS Nano* **16** 3280–9
- [9] Reddy I, Jornet J, Baev A and Prasad P 2020 Extreme local field enhancement by hybrid epsilon-near-zero–plasmon mode in thin films of transparent conductive oxides *Opt. Lett.* **45** 5744–7
- [10] Zhang Y, Gao B, Lepage D, Tong Y, Wang P, Xia W, Niu J, Feng Y, Chen H and Qian H 2024 Large second-order susceptibility from a quantized indium tin oxide monolayer *Nat. Nano* **19** 463–70
- [11] Jiang H *et al* 2023 Thickness-dependent loss-induced failure of an ideal ENZ-enhanced optical response in planar ultrathin transparent conducting oxide films *Opt. Express* **31** 2208–24
- [12] Fujiwara H 2007 *Spectroscopic Ellipsometry Principle and Application* (Wiley, LtdSP)
- [13] Poelman D and Smet P F 2003 Methods for the determination of the optical constants of thin films from single transmission measurements: a critical review *J. Phys. D: Appl. Phys.* **36** 1850–7
- [14] Zhang Z, Hu Y, Lin Z, Si M, Charnas A, Cho K and Ye P D 2022 Atomically thin indium–tin–oxide transistors enabled by atomic layer deposition *IEEE Trans. Electron Devices* **69** 231–6
- [15] Guo E-J, Guo H, Lu H, Jin K, He M and Yang G 2011 Structure and characteristics of ultrathin indium tin oxide films *Appl. Phys. Lett.* **98** 011905
- [16] Li S, Tian M, Gao Q, Wang M, Li T, Hu Q, Li X and Wu Y 2019 Nanometre-thin indium tin oxide for advanced high-performance electronics *Nat. Mater.* **18** 1091–7
- [17] Datta R S *et al* 2020 Flexible two-dimensional indium tin oxide fabricated using a liquid metal printing technique *Nat. Electron.* **3** 51–58
- [18] Si M, Andler J, Lyu X, Niu C, Datta S, Agrawal R and Ye P D 2020 Indium–tin–oxide transistors with one nanometer thick channel and ferroelectric gating *ACS Nano* **14** 11542–7
- [19] Jansen H, Gardeniers H, Boer M D, Elwenspoek M and Fluitman J 1996 A survey on the reactive ion etching of silicon in microtechnology *J. Micromech. Microeng.* **6** 14
- [20] Anopchenko A, Gurung S, Bej S and Lee H 2023 Field enhancement of epsilon-near-zero modes in realistic ultrathin absorbing films *Nanophotonics* **12** 2913–20
- [21] Born M and Wolf E 1999 *Principles of Optics: Electromagnetic Theory of Propagation, Interference, and Diffraction of Light* (Cambridge University)
- [22] Godwin R P and Mueller M M 1973 Reflection spectroscopy by plasma-resonance enhancement *Appl. Opt.* **12** 1276–8

- [23] Harbecke B, Heinz B and Grosse P 1985 Optical properties of thin films and the Berreman effect *Appl. Phys. A* **38** 263–7
- [24] Campione S, Kim I, de Ceglia D, Keeler G A and Luk T S 2016 Experimental verification of epsilon-near-zero plasmon polariton modes in degenerately doped semiconductor nanolayers *Opt. Express* **24** 18782–9
- [25] Berreman D W 1963 Infrared absorption at longitudinal optic frequency in cubic crystal films *Phys. Rev.* **130** 2193–8
- [26] Vassant S, Hugonin J P, Marquier F and Greffet J J 2012 Berreman mode and epsilon near zero mode *Opt. Express* **20** 23971–7
- [27] Xu R *et al* 2024 Highly confined epsilon-near-zero and surface phonon polaritons in SrTiO₃ membranes *Nat. Commun.* **15** 4743
- [28] Ray S, Banerjee R, Basu N, Batabyal A and Barua A 1983 Properties of tin doped indium oxide thin films prepared by magnetron sputtering *J. Appl. Phys.* **54** 3497
- [29] Thompson M W 1968 II. The energy spectrum of ejected atoms during the high energy sputtering of gold *Phil. Mag.* **18** 377–414
- [30] Johansson B O, Sundgren J-E, Hentzell H T G and Karlsson S-E 1984 Influence of substrate shape on tin films prepared by reactive sputtering *Thin Solid Films* **111** 313–22
- [31] Eaton P and West P 2010 *Atomic Force Microscopy* online edn (Oxford Academic)
- [32] May C and Strümpfel J 1999 ITO coating by reactive magnetron sputtering—comparison of properties from DC and MF processing *Thin Solid Films* **351** 48–52
- [33] Higuchi M, Uekusa S, Nakano R and Yokogawa K 1994 Postdeposition annealing influence on sputtered indium tin oxide film characteristics *Jpn. J. Appl. Phys.* **33** 302
- [34] Legeay G and Castel X 2012 A gradual annealing of amorphous sputtered indium tin oxide: crystalline structure and electrical characteristics *Thin Solid Films* **520** 4021–5
- [35] Chan S-H, Li M-C, Wei H-S, Chen S-H and Kuo C-C 2015 The effect of annealing on nanothick indium tin oxide transparent conductive films for touch sensors *J. Nanomater.* **179804** 5
- [36] Ahmed N M, Sabah F A, Abdulgafour H I, Alsadig A, Sulieyman A and Alkhoaryef M 2019 The effect of post annealing temperature on grain size of indium-tin-oxide for optical and electrical properties improvement *Results Phys.* **13** 102159
- [37] Cleary J W, Smith E M, Leedy K D, Grzybowski G and Guo J 2018 Optical and electrical properties of ultra-thin indium tin oxide nanofilms on silicon for infrared photonics *Opt. Mater. Express* **8** 1231–45
- [38] Archer R J I, Passaglia E, Stromberg R R and Kruger J (eds) 1964 *Ellipsometry in the Measurement of Surfaces and Thin Films* (National Bureau of Standards, Misc. Publ., US Government Printing Office) p 256
- [39] Losurdo M *et al* 2009 Spectroscopic ellipsometry and polarimetry for materials and systems analysis at the nanometer scale: state-of-the-art, potential, and perspectives *J. Nanopart. Res.* **11** 1521–54
- [40] Shaltout A M, Shalaev V M and Brongersma M L 2019 Spatiotemporal light control with active metasurfaces *Science* **364** eaat3100
- [41] Novoselov K S, Mishchenko A, Carvalho A and Castro Neto A H 2016 2D materials and van der Waals heterostructures *Science* **353** aac9439
- [42] Ciattoni A, Rizza C, Marini A, Falco A D, Faccio D and Scalora M 2016 Enhanced nonlinear effects in pulse propagation through epsilon-near-zero media *Laser Photon. Rev.* **10** 517–25